Journal of Thermal Analysis and Calorimetry (2020) 141:1331–1339
https://doi.org/10.1007/s10973-019-09121-8

Preparation and properties of negatively charged styrene acrylic latex particles cross-linked with divinylbenzene

Bilge Eren[1] · Yasemin Solmaz[1]

Received: 29 May 2019 / Accepted: 26 November 2019 / Published online: 6 December 2019

Abstract
In this study, the synthesis of divinyl benzene (DVB) cross-linked styrene (Sty)/butyl acrylate (BA)/acrylic acid (AAc) copolymer (SAC) latex particles via the semibatch seeded emulsion polymerization of poly(Sty/BA/AAc) seeds and Sty/BA/AAc or Sty/BA/AAc/DVB monomers was investigated. The structures and morphologies of SAC latex particles were explained by means of DSC, TG/DTG, SEM, ^{1}H-NMR, FTIR, MFFT, and DLS techniques. Optimization studies showed that while the mass ratio of BA in the latex was 68, the glass transition temperature (T_g) value became − 19.8 °C, and when the mass ratio of BA decreased to 30, the T_g value increased to 31.5 °C. The glass transition characteristics of SAC latex were affected by the addition of DVB. The T_g for 0, 0.5, 1.0, 1.5, and 2.0 wt.% DVB/SAC latex particles is 7.5, 8.1, 22.8, 23.4, and 24.5 °C, respectively. The presence of DVB moiety in the SAC latex particles caused the increased thermal stability. The degradation step of the acrylate ester became more dominant with the increasing amount of DVB in the latex. The average particle size and polydispersity index values revealed that the DVB cross-linked SAC latex particles have satisfactory stability and good dispersibility.

Keywords Styrene acrylate copolymer · Cross-linker · Latex · Binder · Seeded polymerization

Introduction

Styrene acrylate copolymer (SAC) latex particles are widely used in water-based wet paint applications, due to their good bonding with substrates, good film-forming properties, hardness, light resistance, stability, and chemical inertness [1–3].

The main application areas for SAC latex are paints [4, 5], coatings [6], inks [7], adhesives [8], and drug delivery [9]. Several studies on SAC latex polymerization have investigated the physical and mechanical properties of latex [10–17]. The film formation of cross-linked latex particles is complex and not well understood due to decreased polymer chain mobility and undesirable phase separation after the cross-linking process [16, 17].

SAC latex with a minimum film formation temperature (MFFT) above room temperature causes undesirable surface defects after coating [18, 19]. For this reason, MFFT values are reduced by the addition of volatile aliphatic or aromatic compounds. However, environmental regulations have been continuously restricting the amount of volatile organic compounds (VOCs) in coatings formulations. For this aim, there is demand to develop the SAC latex to be more compatible with paint additives causing VOC. The recent studies showed that the amount of VOCs can be reduced with cross-linking of the polymer [20–25].

SAC latex particles prepared with AAc has low steric effect, high surface area, high adhesion, high mechanical, and freeze–thaw stabilities and sensitive to pH [16–21]. Divinylbenzene (DVB) is used as a cross-linker in the synthesis of copolymers due to its good mechanical properties and susceptibility to chemical modification [16]. The main strategy of the present work is the preparation of SAC latex particle with negative surface charged and its reaction with DVB. For this aim, Sty/BA/AAc/DVB latex particles were prepared by the method of seeded polymerization. The effect of DVB as a cross-linking agent on the properties of Sty/BA/AAc particle was detailedly studied to understand the nature of the interactions. In order to characterize the prepared latex particles, differential scanning calorimetry (DSC), minimum film formation temperature (MFFT), scanning electron microscopy (SEM), dynamic light scattering

✉ Bilge Eren
bilge.eren@bilecik.edu.tr

[1] Department of Chemistry, Faculty of Science and Arts, Bilecik Seyh Edebali University, 11210 Bilecik, Turkey

(DLS), nuclear magnetic resonance (NMR), and thermal gravimetry (TG) measurements were employed.

Experimental

Materials and instrumentation

The chemical structure of the latex films was characterized by means of infrared spectra (FTIR) recorded in the region 4000–450 cm^{-1} on a Spectrum-100 FTIR spectrometer. Besides, ^{1}H-NMR spectra were recorded with NMR spectrometer (Oxford-NMR300) using choloroform-d_3 as solvent. The thermal gravimetric (TG) and differential thermal analyses (DTA) curves were obtained heating with the rate of 10 °C min^{-1} up to 1000 °C under dry air atmosphere using EXSTAR SII TGA/DTA 7200 TG/DTG apparatus. DSC curves of the latex films were obtained under nitrogen atmosphere between − 50 °C and 100 °C (10 °C min^{-1} heating rate) with PerkinElmer DSC 6000 apparatus. Particle size and morphology of latex particles were recorded using a ZEISS Supra 40 VP model field emission scanning electron microscopy (SEM). Size distribution of the emulsions was determined by intensity with MALVERN Nano-ZS Zeta Potentiometer using DLS method. Minimum Film Formation Temperatures of the latex particles were determined by Rhopoint MFFT 90 device.

Preparation of the latex particles

In the experiments, using the semibatch seeded emulsion process, it was studied with a total mass of 200 g and the total amount of solids (monomers) was 45% (90 g monomer/110 g water). The emulsions were prepared in a 1 L 5-necked water-jacketed reactor, under N_2 medium, using ammonium peroxodisulfate (APS) as initiator and sodium lauryl sulfate (SLS) as emulsifier. Firstly, 95% aqueous initiator solution was prepared by using 0.36 g APS and 6.84 g water, provided that the amount of APS was 0.4% of the total monomer amount. On the other hand, the monomer emulsion was obtained by adding 14.8 g of water (16.5% of monomers), 0.81 g of SLS (0.9% of monomers), 0.33 g of Na_2CO_3 (0.3% of monomers), and BA, Sty, AAc monomers, respectively, with rapid mixing in a Erlenmeyer flask. A mixture of milk consistency is obtained by mixing very fast for approximately 5 h. Monomer ratios of the SAC latex particles prepared (mass%) are given in Table 1. Then, the reactor loading was done. For this, 88.3 g water, 0.72 g (0.8% of monomers) Na_2CO_3, and 0.81 g (0.9% of monomers) SLS were added, respectively, to 1 L 5-necked water-jacketed reactor. The reactor was heated to 80 °C with a circulating water bath by mixing with a mechanical stirrer under nitrogen atmosphere. The semibatch seeded emulsion process consists of two steps, namely seeding and feeding. For seeding, 1.8 g of initiator solution corresponding to 25% of the total followed by certain mass ratio (2.5, 5, 7.5 or 10)% of the monomer emulsion whose total mass is 107 g in each case was added dropwise. The seed ratios of the prepared latex particles were given in the latex codes as brackets. After 30 min of mixing at 400 rpm, the formation of light blue color indicating the formation of nucleation was monitored. Then, remaining initiator solution was added from one of the necks of the reactor, while from the other neck remaining emulsion solution was fed to the system at 80 °C with a peristaltic pump under nitrogen atmosphere for 3 h. After completion of the addition, the system was stirred at 80 °C for a further 1 h and cooled to 30° C with the circulating water bath. DVB cross-linked SAC latex particles were prepared using the same procedure. DVB was added to the monomer emulsion at the feeding stage, and in these latex particles, DVB content was 0.5, 1.0, 1.5, 2.0 mass% of the total monomer mass. The latex films were obtained by pouring a certain amount of the latex onto a glass and evaporation of water at 40 °C in oven (Scheme 1).

Table 1 Reciepes for preparation of SAC latex particles

Latex	BA/ mass%	Sty/ mass%	AAc/ mass%	DVB/ mass%
SAC1(5)	30	68	2	0
SAC2(5)	54	44	2	0
SAC3(5)	59	39	2	0
SAC4(5)	68	30	2	0
SAC2(5)DVB0.5	53.5	44	2	0.5
SAC2(5)DVB1	53	44	2	1
SAC2(5)DVB1.5	52.5	44	2	1.5
SAC2(5)DVB2	52	44	2	2

Result and discussion

Synthesis and characterization of SAC particles

ATR-IR technique was used to determine the structure of the latex samples. The IR spectra showed that all the monomers joined the copolymerization. As shown in Fig. 1, the latex particles exhibited the C–H stretching vibration absorption band of $–CH_3$ and $–CH_3$ groups at 2931, 2958, and 2873 cm^{-1}. The band at 1158 cm^{-1} was assigned to the stretching vibration of C–O–C of ester group in the latex structure [26, 27]. The absorption bands at 3028 and 699 cm^{-1} are characteristic of C–H stretching and C–H out of plane bending of phenyl ring. The bands at 1494, 1452, and 1602 cm^{-1} resulted from the C–C stretching vibration of benzene ring. The band

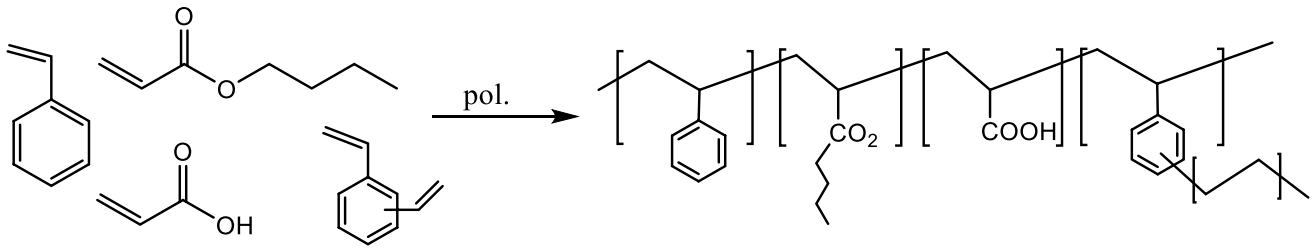

Scheme 1 Preparation of DVB-modified styrene/butyl acrylate/acrylic acid (SAC) latex

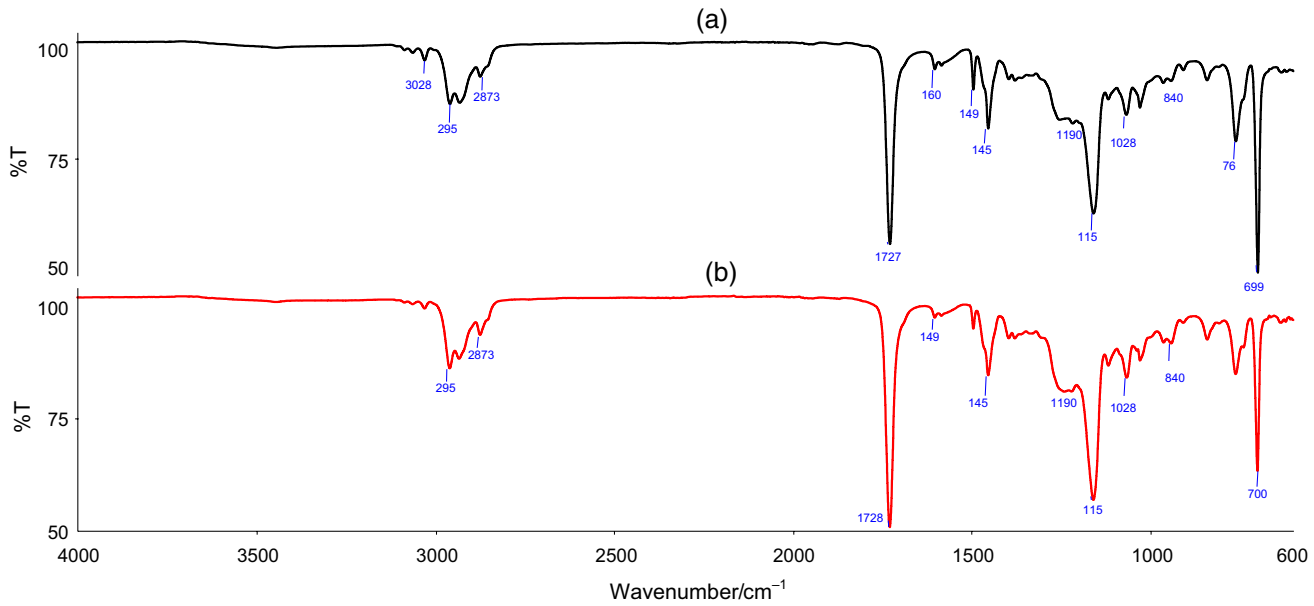

Fig. 1 IR spectra for SAC2(5) (a) and SAC2(5)DVB1 particles (b)

at 760 cm^{-1} corresponding to aromatic C–H bending of the phenyl ring was broadened after DVB cross-linking process. The characteristic C–O stretching vibration band of AAc moiety was observed at 1190 cm^{-1} [27]. The distorted band at 1728 cm^{-1} is due to the overlapping carbonyl stretching vibrations of AAc (1705 cm^{-1}) and BA (1730 cm^{-1}).

The representative ^{1}H-NMR spectrum of SAC2(5) latex is shown in Fig. 2. The peak assignments of the protons in the structure are given on the spectrum. As shown in Fig. 2, the phenyl groups of Sty units in the polymer are located at ~6.75–7.26 ppm. The –OCH_2– groups of BA units in the polymer are located at ~3.79 ppm [28]. The signal group at 0.87–2.21 ppm stands for the protons on the polymer backbone. The signal of the hydrogen in carboxyl groups is not observed due to chemical exchange [29]. These results indicate that the monomers are successfully transformed to the latex during polymerization.

Thermal properties of latex particles

As shown in Fig. 3, one characteristic endothermic shift was observed on the DSC curves of SAC latex particles. It is known that the T_g values for homopolymers of BA and Sty are − 54 °C and 105 °C, respectively. As given in Table 2, the T_g values of SAC samples increased from − 19.8 to 31.5 °C with increasing Sty amount from 30 to 68%.

The T_g of the latex can be calculated using the Fox equation [30] (Eq 1):

$$1/T_g\ (\text{Latex}) = W(a)/T_g(a) + W(b)/T_g(b) + \cdots \quad (1)$$

where $W(a)$ and $W(b)$ are the mass ratio of monomers (a) and (b) and T_g (a) and T_g (b) are the glass transition temperatures for homopolymers (a) and (b), respectively.

The theoretical T_gs calculated by Fox equation is 37.4, − 1.4, − 8.4, and − 19.9 °C, and the T_gs tested in our

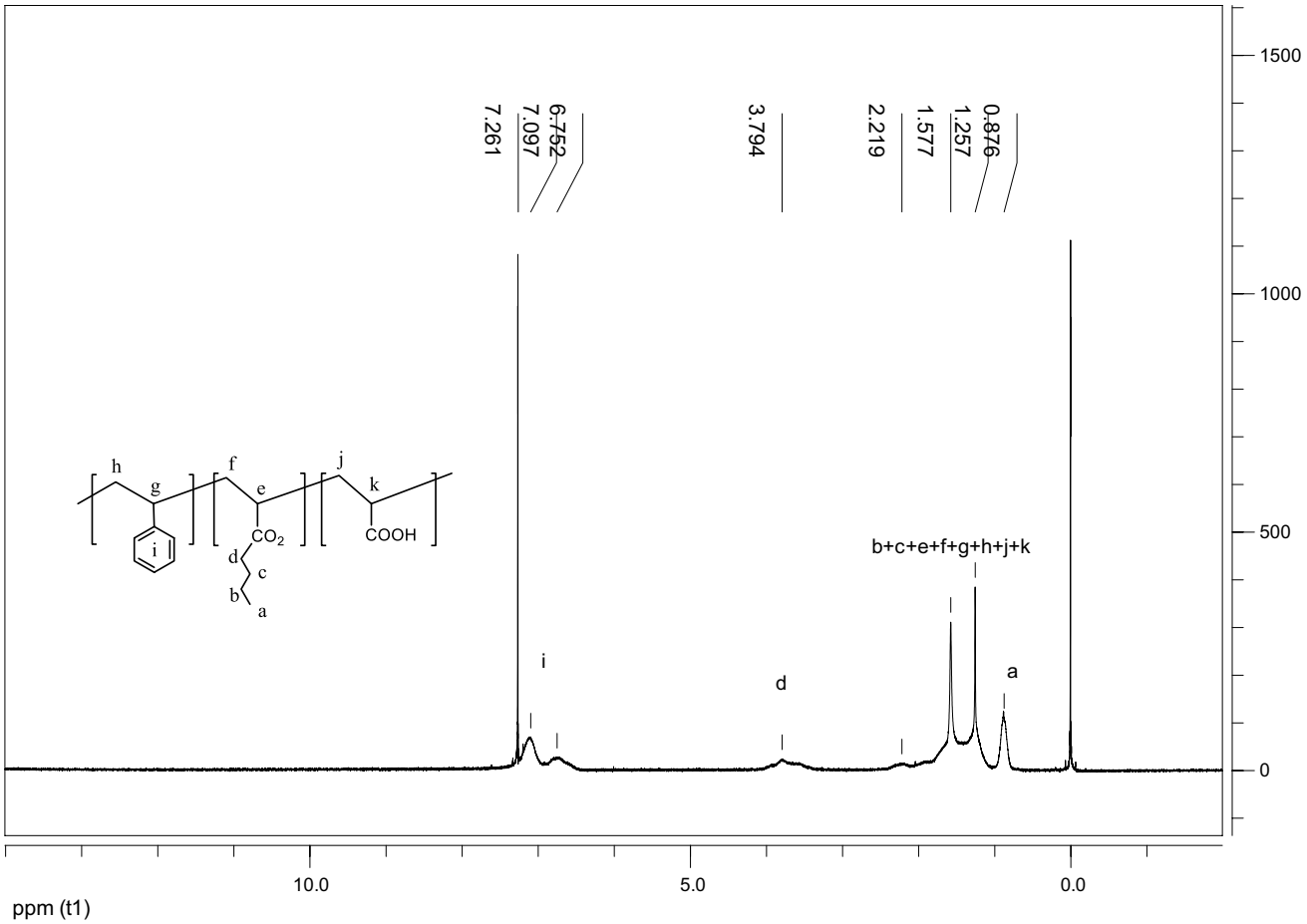

Fig. 2 ^{1}H-NMR spectrum of SAC2(5) latex film in chloroform-d_3

experiment is 31.5, 7.5, − 5.6, and − 19.8 °C (Table 2). DSC curves of the SAC latex particles prepared from different seed mass ratio varied from 2.5 to 10% are, respectively, shown in Fig. 4. As shown in Fig. 4, the T_g values decreased with increasing the amount of seed in the latex. For example, while the mass ratio of seed in the latex was 10%, T_g was − 0.7 °C, and when the ratio of seed decreased to 2.5%, the T_g increased to 17.5 °C. The low T_g values may be related to the easier migration of BA monomer into the surfactant micelle for polymerization at the seed surface [31] and also the large diameter of the latex seed causing the growth of a large number of BA on SAC backbone.

The effect of DVB amount as the cross-linker was also examined (Fig. 5 and Table 3). DVB is commonly used as a cross-linking agent to help increase the hardness and robustness of a polymer [16, 32]. The T_g of SAC2(5) latex particle was determined to be at 7.5 °C. The T_g of DVB cross-linked SAC2(5) increased with DVB content in the latex. The increase in T_g is due to the reduction in molecular mobility of polymer chain in the presence of DVB moiety in polymer backbone.

As given in Table 3, the DVB content in the latex also affected the film formation. It could be said that MFFT values increased with the increasing amount of DVB. In the presence of 1–2 mass% DVB, MFFT values of the latexes changed between 0 and 9 °C. MFFT value of DVB cross-linked SAC latex is lower than its T_g value. This result indicates that the DVB content in the latex affects the latex hardness/softness properties that also strongly affect the film formation.

Thermal stability of the latex particles

In order to define the thermal stability of the latex particles, it is necessary to know their degradation temperature. For this reason, a series of temperatures have been defined: $T_{10\%}$ (temperature at which 10% of the initial mass is lost), $T_{50\%}$ (temperature at which 50% of the initial mass is lost), T_{max} (temperature at the maximum rate of thermal decomposition), and $(dw/dt)_{max}$ (maximum mass loss at T_{max}). As shown in Table 4, all the experimental data of SAC latex particles displayed comparable trend (Fig. 6). The $T_{10\%}$ of

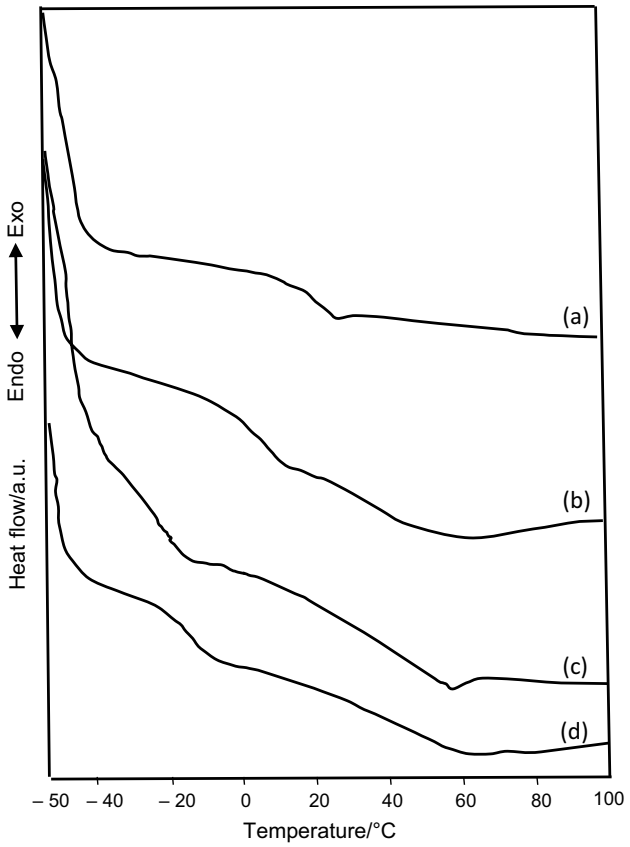

Fig. 3 DSC curves for SAC particles. SAC1(5) (a), SAC2(5) (b), SAC3(5) (c), and SAC4(5) (d)

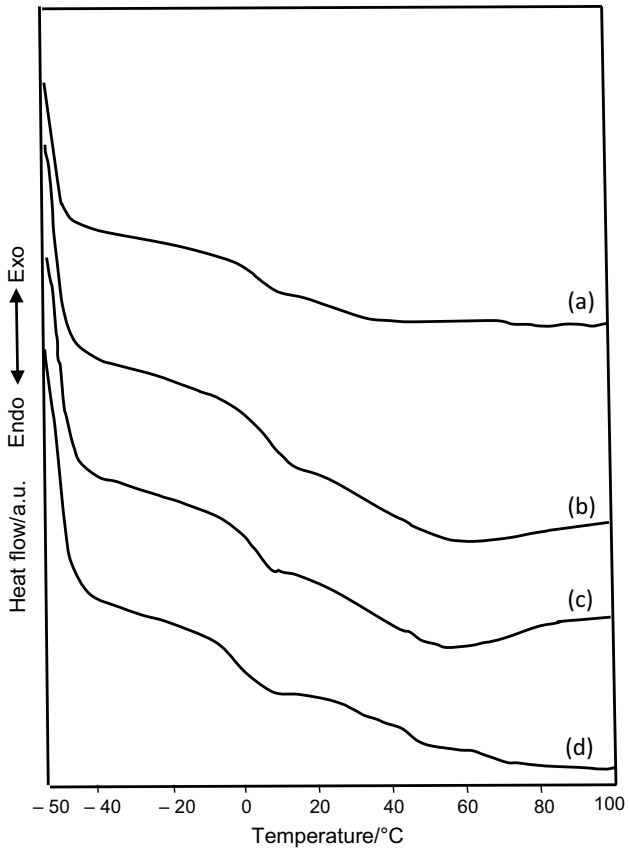

Fig. 4 DSC curves of SAC2 particles with seed mass ratios of 2.5 (a), 5 (b), 7.5 (c), and 10 (d)

Table 2 T_g, MFFT, and average particle size values for SAC latex particles with various monomer contents

Latex	T_g/°C		MFFT/°C	Average particle size/nm	
	Exp.	Fox eq.		SEM	DLS
SAC1(5)	31.5	37.4	26.3	80	87.43
SAC2(5)	7.5	– 1.4	5.0	109	118.30
SAC3(5)	– 5.6	– 8.4	1.0	95	97.03
SAC4(5)	– 19.8	– 19.9	1.0	–	92.64

SAC1(5) was 357 °C. By adding more BA into emulsion, the $T_{10\%}$ of latex continuously decreased to 332, 329, and 328 °C for SAC2(5), SAC3(5), and SAC4(5) latex particles, respectively (Table 4).

As given in Table 5, the TG curves for all the latex samples contained three separated degradation stages. This result points out that the formation of the DVB cross-linked networks did not change the thermal degradation behavior of the SAC latex. The moisture absorbed by the latex was lost during these first stages of the thermal decomposition. The second decomposition stage was observed in the range of 190–650 °C with the maximum mass loss (T_{max2}) at 400–405 °C. The third decomposition stage took place between ~ 650 and 935 °C with T_{max3} at 714–719 °C (Table 5). The second decomposition stage could be associated with the ester bonds breakdown in latex particles, and the third one could be attributed to the total degradation of copolymers [32]. The results in Table 5 showed that the degradation step of the acrylate ester became more dominant with the increasing amount of DVB in the latex. For this reason, the thermal stability of latex was determined from second-stage mass loss in the TG curve. The results indicated that the cross-linking of DVB affects the thermal stability of the latex. The obtained $T_{10\%}$ and $T_{50\%}$ values showed an increase in the thermal stability of latex particles (Table 5). The increase in the stability of the SAC latex becomes evident with DVB content of 1% and more. In the presence of 1–2 mass% DVB, the thermal stability of the latex was

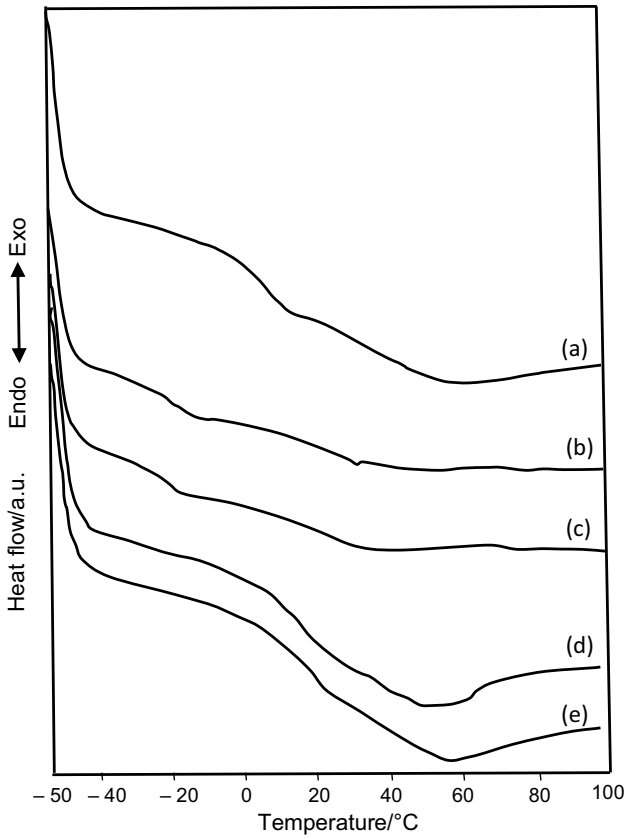

Fig. 5 DCS curves of SAC2(5) particles cross-linked with 0 (a), 0.5 (b), 1.0 (c), 1.5 (d), and 2.0% DVB (e)

Table 3 T_g, MFFT, and average particle size, and polydispersity index values for the DVB cross-linked SAC latexes

Latex	T_g/°C	MFFT/°C	Average particle size/nm		PDI
			SEM	DLS	
SAC2(5)	7.5	5.0	109	118.30	0.150
SAC2(5)DVB0.5	8.1	0	96	131.20	0.015
SAC2(5)DVB1	22.8	0.1	98	83.62	0.074
SAC2(5)DVB1.5	23.4	9.0	151	194.60	0.109
SAC2(5)DVB2	24.5	5.0	123	122.60	0.140

Table 4 TG characteristics for latex particles with different monomer amounts

Latex	T_{max}/°C	$(dw/dt)_{max}$/% min^{-1}	$T_{10\%}$/°C	$T_{50\%}$/°C
SAC1(5)	75	0.37	357	399
	404	23.18		
	712	0.042		
SAC2(5)	71	0.32	332	384
	405	18.66		
	716	0.72		
SAC3(5)	95	0.36	329	381
	388	15.81		
	676	0.33		
SAC4(5)	47	0.36	328	378
	385	15.60		
	555	0.52		

increased by 10–15 °C. It is seen that in the presence of DVB content of more than 1.5 mass%, the breakdown of the acrylate ester networks in the copolymer chain becomes more dominant (T_{max2} degradation rate 21.1% min^{-1}).

SAC latex was found to be thermally stable up to 716 °C, while the cross-linked SAC latex particles containing 0.5, 1.0, 1.5, and 2.0% DVB were thermally stable up to 719, 719, 714, and 714 °C, respectively. It is seen that the $(dw/dt)_{max}$ for all samples at all degradation stages fluctuated with increasing DVB content (Table 5). This result may be attributed to the width of the particle size distribution increased with the addition of DVB. The smallest particles are more exposed to the thermal degradation because of their larger superficial area [33].

Particle size and morphology of the latex particles

The effect of DVB amount on particle size has been investigated using DLS and SEM techniques. To our knowledge, no prior studies have examined the particle size distribution of DVB cross-linked Sty/BA/AAc copolymer latex particles. The particle size distribution obtained from DLS measurements for the SAC latex particles with different DVB amount is given in Table 3.

DVB is a more hydrophobic and reactive monomer than styrene [34, 35]. It reacts in the early stages of polymerization [34] and ensures lower interfacial tension and smaller

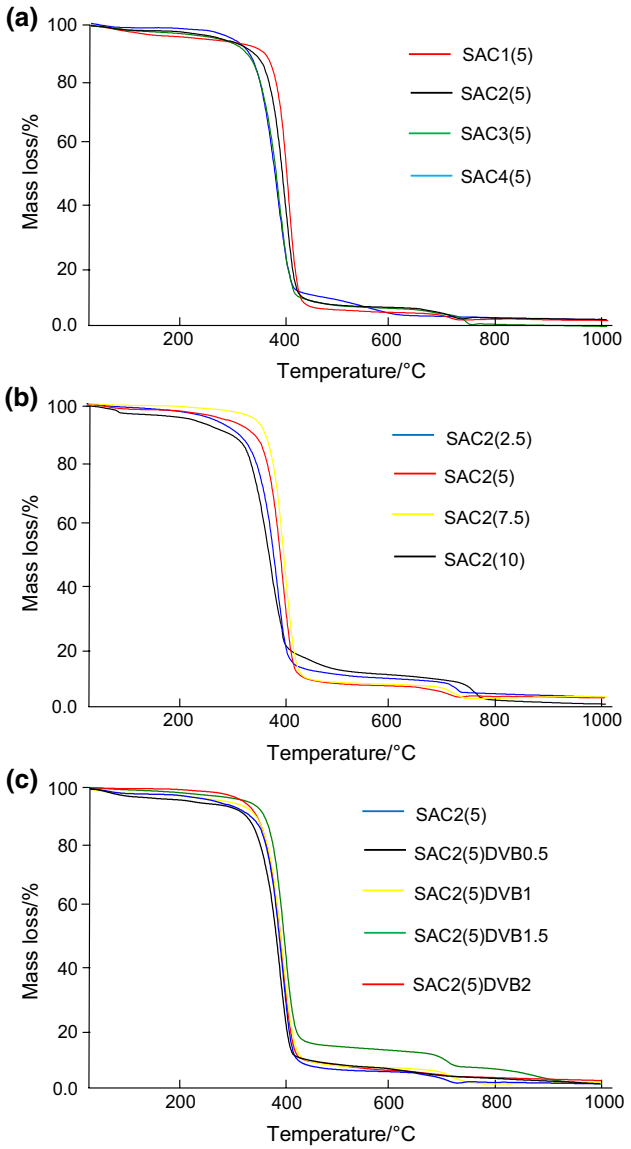

Fig. 6 TG curves for SAC particles with different monomer (**a**), seed (**b**), and DVB amount (**c**)

droplet size [35]. The average particle size (obtained from DLS measurements) fluctuated between 83.62 and 194.60 nm with the increase in the amount of DVB. This result can be concluded that the shape of the particle changed from sphere to irregular spheroid such as ellipsoid, snowman, dumbbell, and trimer among others due to the different reactivities of DVB and styrene [36].

Table 5 TG characteristics of various amounts of DVB cross-linked SAC latex particles

Latex	T_{max}/ °C	$(dw/dt)_{max}$/% min^{-1}	$T_{10\%}$/°C	$T_{50\%}$/°C
SAC2(5)	71	0.32	332	384
	405	18.66		
	716	0.72		
SAC2(5)DVB0.5	72	0.47	332	389
	400	18.34		
	719	0.82		
SAC2(5)DVB1	47	0.26	348	395
	400	17.81		
	719	0.90		
SAC2(5)DVB1.5	70	0.30	344	399
	402	21.11		
	714	0.80		
SAC2(5)DVB2	54	0.1	347	392
	401	21.13		
	714	0.80		

The polydispersity index (PDI) is a measure of dispersion homogeneity and ranges from 0 to 1. Values close to 0 indicate a homogeneous dispersion, while those > 0.3 indicate high heterogeneity [37]. The PDI values for DVB cross-linked SAC particles varied between 0.015 and 0.140 which correspond to quite homogenous distributions (Table 3).

The PDI increased from 0.015 to 0.140 for DVB contents of 0.5, and 2%, respectively. The increasing PDI values showed a second nucleation and particle coagulation [36]. The monomer molecules having different reactivity in the micelle phase reacted in different stages of polymerization, leading to the second nucleation.

The SAC latex particle structures were investigated using SEM technique. As shown in Fig. 7, the SEM analysis of the SAC particles confirmed the results obtained from the DLS measurement. The average particle diameter obtained from SEM was changed in the range of 96 nm and 151 nm, which is nearly same with the DLS data.

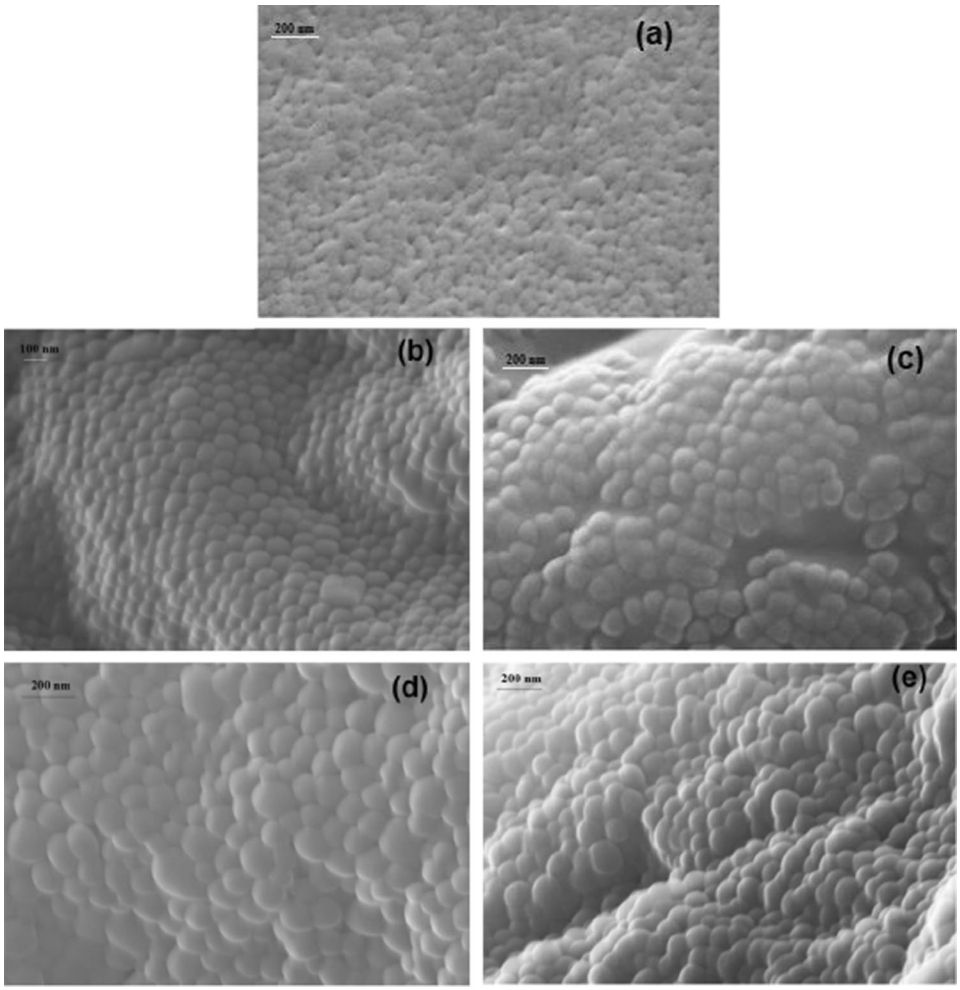

Fig. 7 SEM images of SAC2(5) particles cross-linked with 0 (**a**), 0.5 (**b**), 1.0 (**c**), 1.5 (**d**), and 2.0% DVB (**e**)

Conclusions

All of the SAC latex particles exhibited only one T_g, indicating that all the monomers had participated in the reaction to form latex, and there was no homopolymer occurred during the polymerization. The measured value of T_g is very close to its theoretical value calculated by Fox equation. The average particle size values obtained by DLS technique are consistent with the values obtained from the SEM images. The average particle size and PDI for SAC emulsion without DVB were 118.30 nm and 0.150, respectively, indicating good stability and dispersibility. When the DVB content was increased to 2.0%, the particle sizes of latex particles was 122.60 nm and PDI was 0.140, which indicated satisfactory latex stability.

Acknowledgements This study was supported by Bilecik Şeyh Edebali University with the project number of 2018-01.BŞEÜ.04-07. Authors also thank to DYO Boya Fabrikaları Sanayi ve Ticaret A.Ş., İzmir for MFFT and DSC analysis of the polymers.

References

1. Qiu XL, Lu LX, Han PJ, Tang GY, Song GL. Fabrication, thermal property and thermal reliability of microencapsulated paraffin with ethyl methacrylate-based copolymer shell. J Therm Anal Calorim. 2016;124:1291–9.
2. Lopez-Beceiro J, Alvarez-Garcia A, Martins S, Alvarez-Garcia B, Zaragoza-Fernandez S, Menendez-Valdes J, Artiaga R. Thermal degradation kinetics of two acrylic-based copolymers. J Therm Anal Calorim. 2015;119:1981–93.
3. Nguyen TT, Xiao ZF, Che WB, Trinh HM, Xie YJ. Effects of modification with a combination of styrene-acrylic copolymer dispersion and sodium silicate on the mechanical properties of wood. J Wood Sci. 2019. https://doi.org/10.1186/s10086-019-1783-7.
4. Ray NK, Gundabala V. Synthesis and characterization of titanium dioxide encapsulated poly (styrene-co-butyl acrylate-co-acrylic acid) nanocomposite latex. Prog Org Coat. 2017;111:93–8.
5. Ramde T, Ecco LG, Rossi S. Visual appearance durability as function of natural and accelerated ageing of electrophoretic styrene-acrylic coatings: influence of yellow pigment concentration. Prog Org Coat. 2017;103:23–32.
6. Grigsby WJ. Photooxidative stability provided by condensed tannin additives in acrylic-based surface coatings on exterior exposure. J Coat Technol Res. 2018;15:1273–82.

7. Ataeefard M. Preparing nanosilver/styrene-butyl acrylate core-shell composite via eco-friendly emulsion aggregation method as a printing ink. Colloid Polym Sci. 2018;296:819–27.
8. Anjana S, Jayaram RV. A comparative study of properties of acrylic based water-borne polymers using various surfactants for adhesive applications. Polym Sci Ser B+. 2018;60:629–37.
9. Rajaee A, Farzi G. Encapsulation of paclitaxel in ultra-fine nanoparticles of acrylic/styrene terpolymer for controlled release. Colloid Polym Sci. 2016;294:95–105.
10. Limousin E, Ballard N, Asua JM. The influence of particle morphology on the structure and mechanical properties of films cast from hybrid latexes. Prog Org Coat. 2019;129:69–76.
11. Abdel-Rahman HA, Younes MM, Khatta MM. Effect of waste glass content on the physico-chemical and mechanical properties of styrene acrylic ester blended cement mortar composites. Polym Polym Compos. 2018;39:985–96.
12. Barata I, Fonseca AC, Costa CSMF, Ferreira L, Julio E, Coelho JFJ. Insights into the thermo-mechanical properties of films cast from emulsion terpolymers. Prog Org Coat. 2014;77:790–7.
13. Pacheco-Salazar OF, Wakayama S, Sakai T, Rios-Soberanis CR, Cauich-Rodriguez JV, Cervantes-Uc JM. Damage accumulation studied by acoustic emission in bone cement prepared with core-shell nanoparticles under fatigue. J Mater Sci. 2016;51:5635–45.
14. Shao-Jie L, Qian-Qian H, Feng-Qing Z, Xiao-Menga C. Utilization of steel slag, iron tailings and fly ash as aggregates to prepare a polymer-modified waterproof mortar with a core-shell styrene-acrylic copolymer as the modifier. Constr Build Mater. 2014;72:15–22.
15. Wang FZ, Luo YW, Li BG, Zhu SP. Synthesis and redispersibility of poly(styrene-block-n-butyl acrylate) core-shell latexes by emulsion polymerization with RAFT agent-surfactant design. Macromolecules. 2015;48:1313–9.
16. Jaiswal KK, Manikandan D, Murugan R, Ramaswamy AP. Microwave-assisted rapid synthesis of Fe_3O_4/poly(styrene-divinylbenzene-acrylic acid) polymeric magnetic composites and investigation of their structural and magnetic properties. Eur Polym J. 2018;98:177–90.
17. Yu FY, Fang Y, Wang JJ, Xu YL, Shi J. Fabrication of compact poly(methyl methacrylate-co-butyl methacrylate-co-acrylic acid) microcapsules for electrophoretic displays by using emulsion droplets as templates. Colloid Polym Sci. 2016;294:1359–67.
18. Stewarda PA, Hearna JU, Wilkinson MC. An overview of polymer latex film formation and properties. Adv Colloid Interface. 2000;86:195–267.
19. Kumthekar V, Kolekar S. Attributes of the latex emulsion processing and its role in morphology and performance in paints. Prog Org Coat. 2011;72:380–6.
20. Mori H, Muller AHE. New polymeric architectures with (meth) acrylic acid segments. Prog Polym Sci. 2003;28:1403–39.
21. Trojer MA, Nordstierna L, Bergek J, Blanck H, Holmberg K, Nydéna M. Use of microcapsules as controlled release devices for coatings. Colloid Interface. 2015;222:18–43.
22. Srivastava S. Co-polymerization of Acrylates. Des Monomers Polym. 2009;12:1–18.
23. Wicks ZW, Wicks DA, Rosthauser JW. Two package waterborne urethane systems. Prog Org Coat. 2002;44:161–83.
24. He M, Xu J, Qiu F, Chen X. Preparation, characterization, and property analysis of environmentally friendly waterborne polyurethane-acrylate. Int J Polym Anal Charact. 2013;18:211–23.
25. Huybrechts J, Bruylants P, Vaes A, Marre AD. Surfactant-free emulsions for waterborne, two-component polyurethane coatings. Prog Org Coat. 2000;38:67–77.
26. Hongwei Z, Songnan N, Yonghua L. Characteristics of styrene-acrylate micro emulsion with high solid content and their effect on the coating properties. Adv Mater Res. 2013;791–793:44–7.
27. Inas AMJ, Ammar AAH, Rizgar MAH. Fourier transform infrared (FT-IR) spectroscopy of modified heat cured acrylic resin denture base material. IJERSTE. 2015;5:172–80.
28. Stéphane R, Marc AD. Emulsion-based pressure sensitive adhesives from conjugated linoleic acid/styrene/butylacrylate terpolymers. Int J Adhes Adhes. 2016;70:17–25.
29. Shimou C, Guozhong W, Yaodong L, Dewu L. Preparation of poly(acrylic acid) grafted multiwalled carbon nanotubes by a two-step irradiation technique. Macromolecules. 2006;39:330–4.
30. Fox TG. Influence of diluent and copolymer composition on the glass temperature of a polymer system. Bull Am Phys Soc. 1956;1:123–8.
31. Nuasaen S, Tangboriboonrat P. Highly charged hollow latex particles prepared via seeded emulsion polymerization. J Colloid Interface Sci. 2013;396:75–82.
32. Podkoscielna B, Worzakowska M. Synthesis, characterization, and thermal properties of diacrylic/divinylbenzene copolymers. J Therm Anal Calorim. 2010;101:235–41.
33. Villanova JCO, Ayres E, Carvalho SM, Patrício PS, Pereirad FV, Oréfice RL. Pharmaceutical acrylic beads obtained by suspension polymerization containing cellulose nanowhiskers as excipient for drug delivery. Eur J Pharm Sci. 2011;42:406–15.
34. Shim S-E, Cha Y-J, Byun J-M, Choe S. Size control of polystyrene beads by multistage seeded emulsion polymerization. Appl Polym. 1999;71:2259–69.
35. Cameron NR. High internal phase emulsion templating as a route to well-defined porous polymers. Polymer. 2005;46:1439–49.
36. Liu B, Sun S, Zhang M, Zhang H. Synthesis of large-scale, narrowly dispersed, highly cross-linked, and spherical latex particles via one-step emulsion polymerization through particle coagulation. J Dispers Sci Technol. 2017;38:1147–53.
37. Wang W, Zhang Q. Synthesis of block copolymer poly (n-butyl acrylate)-b-polystyrene by DPE seeded emulsion polymerization with monodisperse latex particles and morphology of self-assembly film surface. J Colloid Interface Sci. 2012;374:54–60.